iScience

CellPress
OPEN ACCESS

Article

Type I interferon signaling regulates myeloid and T cell crosstalk in the glioblastoma tumor microenvironment

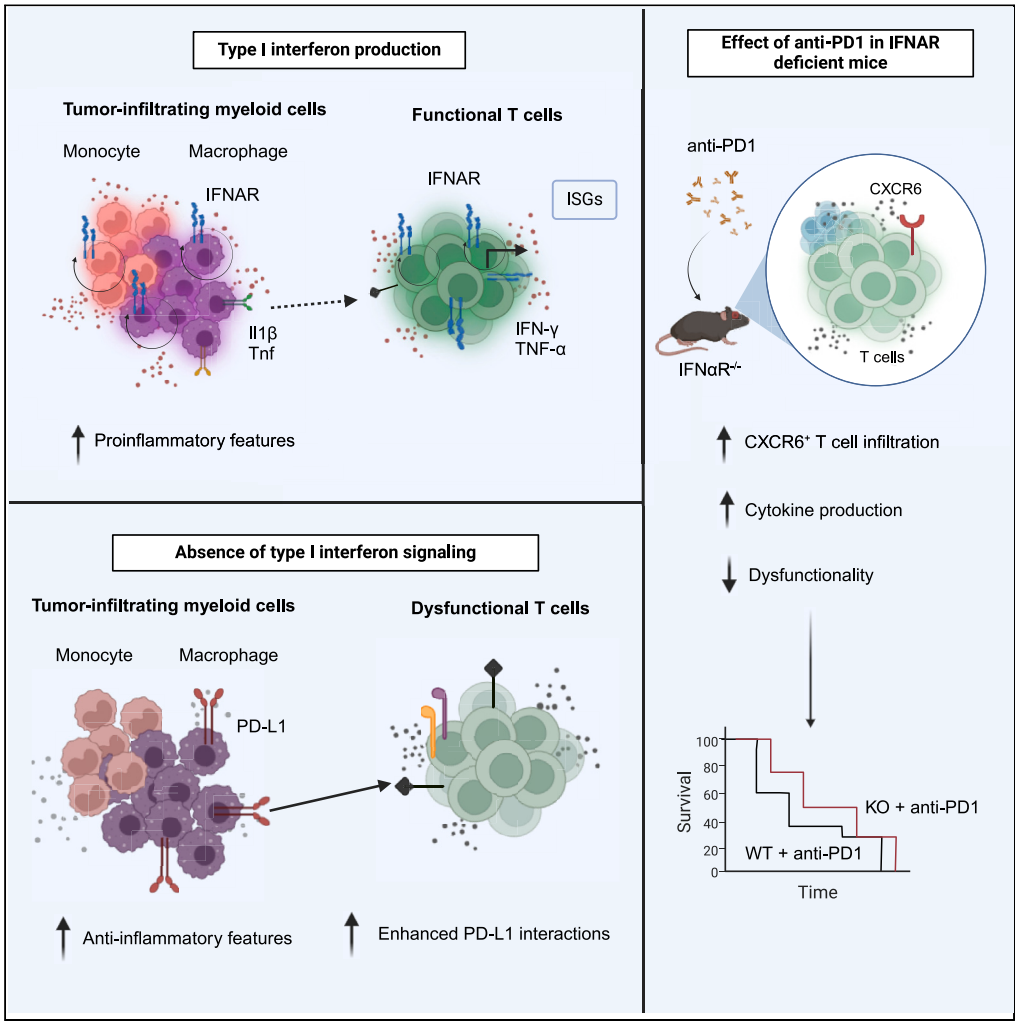

Juhee Lim, Jeongwoo La, Hyeon Cheol Kim, ..., Yumin Kim, Myoung Seung Kwon, Heung Kyu Lee

heungkyu.lee@kaist.ac.kr

Highlights

Myeloid cells highly contribute to type I IFN production in the GBM TME

Absence of type I IFN signaling induces an M2 signature in macrophages

PD-L1 interactions are enhanced in absence of type I IFN production

Anti-PD1 enhances CXCR6^{+} CD8 T cell infiltration in IFNαR$^{-/-}$ mice

Lim et al., iScience 27, 110810
September 20, 2024
https://doi.org/10.1016/j.isci.2024.110810

iScience

CellPress
OPEN ACCESS

Article

Type I interferon signaling regulates myeloid and T cell crosstalk in the glioblastoma tumor microenvironment

Juhee Lim,[1] Jeongwoo La,[1,2] Hyeon Cheol Kim,[2,3] In Kang,[1,2] Byeong Hoon Kang,[1,2] Keun Bon Ku,[1,2,4] Yumin Kim,[2] Myoung Seung Kwon,[1,2] and Heung Kyu Lee[2,5,6,*]

SUMMARY

Downstream interferon signaling through the type I interferon (IFN) receptor, IFNAR, is crucial for the proper production of type I IFNs in mounting anti-tumor immune responses. Our study investigates the role of type I IFN signaling in the glioblastoma (GBM) tumor microenvironment by leveraging single-cell RNA sequencing to analyze tumor-infiltrating lymphocytes. We investigate how type I IFN signaling within the myeloid compartment contributes to the crosstalk with T cells in the tumor microenvironment. Through the use of the GI261 murine GBM model, we find that the lack of proper type I IFN response results in enhanced PD-L1 interactions among myeloid cells, thereby affecting T cell functionality. Additionally, we also characterize how anti-PD1 treatment induces transcriptional changes in tumor-associated monocytes and macrophages by analyzing intercellular communication networks and propose how immune checkpoint blockade therapy could possibly relieve some of the immunosuppression derived from the lack of proper type I IFN production.

INTRODUCTION

Glioblastoma (GBM) is the most devastating and aggressive form of brain tumor.[1] Despite therapeutic advances in cancer immunotherapy, GBM remains one of the most treatment-resistant tumors.[2] Due to the intratumoral heterogeneity, conventional and molecular targeted therapies are met with limited success.[3] Recently, strategies introducing immune-activating cytokines to the tumor microenvironment (TME) through gene and cell-based delivery systems have been shown to reprogram the TME and enhance immune responses against GBM. Among the several immune-activating cytokines that have been delivered to the TME, delivery of IFN-α has shown therapeutic benefits by alleviating T cell exhaustion and reprogramming the myeloid compartment toward a proinflammatory phenotype.[4] It is able to block tumor cell progression by preventing cell-cycle progression and triggering apoptosis.[5] Type I IFNs are a family of cytokines that intervene in all phases of the cancer immunoediting process.[6] Production of type I IFNs in the tumor microenvironment enhances cytotoxic functions of effector T cells, contributes to the activation and maturation of dendritic cells, and leads to better antigen-presenting and processing for T cell priming and activation.[7] Thus, type I IFN signatures are considered favorable biomarkers of immune response and also good prognostic markers in determining response to immunotherapy.[8]

Immune checkpoint blockade has revolutionized the cancer oncology field, yet there are still hurdles that need to be overcome.[9] The main mechanism of action of checkpoint inhibitors is controlling tumor progression by blocking inhibitory signals of T cell activation through the use of immune checkpoint inhibitors.[10] Studies have shown that temporal type I IFN signaling is critical for effective response to immune checkpoint therapy and IFN response gene signatures predict improved immunotherapy outcomes.[11–13]

While a number of studies suggest an association between type I IFN signature and positive response to immune checkpoint blockade, some contradicting studies suggest a protumoral role for type I IFNs. For example, a recent study hypothesized that the sustained production of type I IFNs promotes tumor growth and resistance to immune checkpoint blockade therapy.[14] In addition, tumor-derived type I IFN signaling was shown to drive cancer stemness by inducing the release of cancer-derived exosomes with high expression levels of immune checkpoint receptor ligands, ultimately leading to T cell exhaustion, and therefore, predicting a poor response to immunotherapy.[15] Thus, there are divided opinions regarding whether type I IFNs exert anti-tumoral or protumoral effects.

There has not been much study done assessing the qualitative changes induced in the tumor microenvironment through type I IFN signaling. Here, we provide a detailed analysis of the GBM TME by leveraging single-cell RNA sequencing (scRNA-seq) analysis and provide a transcriptional characterization of immune cells that have been affected by a lack of proper type I IFN production. Our study shows that type

[1]Graduate School of Medical Science and Engineering, Korea Advanced Institute of Science and Technology (KAIST), Daejeon 34141, Republic of Korea
[2]Laboratory of Host Defenses, Department of Biological Sciences, KAIST, Daejeon 34141, Republic of Korea
[3]Life Science Institute, KAIST, Daejeon 34141, Republic of Korea
[4]Center for Infectious Disease Vaccine and Diagnosis Innovation, Korea Research Institute of Chemical Technology, Daejeon 34114, Republic of Korea
[5]KAIST Institute of Health Science and Technology, KAIST, Daejeon 34141, Republic of Korea
[6]Lead contact
*Correspondence: heungkyu.lee@kaist.ac.kr
https://doi.org/10.1016/j.isci.2024.110810

I IFNs regulate interactions between myeloid cells and T cells by inducing transcriptional and functional changes. We also see that the administration of immune checkpoint inhibitors may contribute to the restoration of immune cell function even in the absence of type I IFN signaling.

RESULTS

Analysis of newly diagnosed patients with glioblastoma reveals the expression of interferon-stimulated genes in tumor-infiltrating myeloid cells

To explore the status of type I IFN signaling in human gliomas, we analyzed public data of a newly diagnosed GBM patient sample (GSE182109).[16] We were able to identify multiple immune cell types based on expression of major markers: microglia (*TMEM119*), monocytes (*CD14, CD16*), T cells (*CD3E*), macrophages (*SIGLEC1, CD68*), proliferating cells (*MKI67*), stem cells (*COX7A1*), endothelial cells (*PROX1*), dendritic cells (*ZBTB20*), and glial cells (*PLP1, APLP1*) (Figure 1A; Figure S1A). While type I IFNs are produced by most nucleated cells, their signaling is mediated through a common cell surface type I receptor complex composed of two subunits, IFNAR1 and IFNAR2.[17] We analyzed expression of *IFNAR1* and *IFNAR2,* and saw that intratumoral microglia, monocytes, and macrophages showed high expression of both receptor subunits, indicating a rich capacity for IFN signaling (Figure 1B).

Downstream type I IFN signaling leads to the expression of interferon-stimulated genes (ISGs) that often predict response to cancer immunotherapy.[18] They form the backbone of the innate immune system and studies conducted in virus studies have suggested high responsiveness of tumor-infiltrating myeloid cells to type I IFNs.[19,20] Thus, we assessed the expression of several ISGs (*CAMK2G*, *EIF4A2*, *EIF4G3*, *FLNB*, *RPS27A*, *KPNA3*, *NUP133*, *JAK2*, *GBP7*, *TRIM3)* which were highly expressed among tumor-infiltrating monocytes, microglia, and macrophages (Figure 1C). Each individual ISG that was expressed among these myeloid cells was associated with increased GBM patient survival based on The Cancer Genome Atlas (TCGA) (Figure S1C).

We were able to derive an ISG signature score to assess type I IFN pathway engagement across cell types based on the ISGs that were expressed specifically within the myeloid compartment. This ISG signature score was the highest, particularly among tumor-infiltrating myeloid cells (Figure 1D). Using this ISG signature, we assessed the survival of patients with LGG and GBM from the TCGA database. We saw that there was an association between a high myeloid ISG signature and increased human patient survival (Figure 1E), suggesting that type I IFN signaling among the myeloid compartment of the GBM TME contributes to the overall survival of patients with GBM. Identifying the source of type I IFNs is difficult because the direct detection of type I IFNs has been proven challenging.[21] However, previous research has shown that the absence of IRF-3 still maintains a weak type I IFN response, but IRF-7 is indispensable for type I IFN production.[22] We saw that *Irf3* expression was spread across lymphoid cells for both humans and mice. On the other hand, *Irf7* was highly expressed among tumor-infiltrating myeloid cells (Figures S1B and S2D). This corroborates our conclusions suggesting that the myeloid compartment highly contributes to the maintenance of type I IFN signaling.

Perturbation of interferon signaling reduces glioblastoma survival and induces changes in the myeloid compartment

In order to assess the contribution of type I IFN signaling in antitumor responses we used the orthotopic Gl261 mouse glioma model. We injected Gl261 GBM cells in mice that were deficient for IFNAR (IFN$\alpha R^{-/-}$). We found that the absence of the IFNAR reduced the survival rate against GBM (Figures 2A and 2B). To determine changes in the immune landscape of the GBM TME in the absence of proper type I IFN signaling, we performed scRNA-seq on CD45.2^{+} tumor-infiltrating immune cells from mouse brains collected 20 days post Gl261 implantation (Figure S2A). We were able to confirm the deficiency of IFNAR by the overall decreased expression of ISGs (Figure S2C). UMAP analysis showed distinct populations of myeloid and lymphoid cells (Figure S2B) and reduced infiltration of immune cells into the tumor microenvironment in the absence of IFNAR (Figure 2C). Major cell types were identified based on expression of major markers: T cells (*Cd3e, Cd8a, Cd4*), NK cells (*Ncr1, Klrk1*), microglia (*Tmem119, Siglech*), dendritic cells (*Ccr7, Mreg, H2-DMb2, Fscn1*), monocytes and macrophages (*Cd14, Clec4n*), plasmacytoid dendritic cells (*Ccr9, Spib*), mast cells and basophils (*Gata2, Cd200r3*), and neutrophils (*S100a9, S100a8*) (Figure 2D). To investigate qualitative changes induced by the absence of proper type I IFN signaling, we analyzed the differentially expressed genes (DEGs) among total immune cells. Quantification of DEGs among each immune cell subset showed the highest number of DEGs among tumor-infiltrating monocytes and macrophages (Figure 2E). By using the top 15 highest upregulated and downregulated DEGs between WT and IFN$\alpha R^{-/-}$ mice, we derived DEG signature scores and saw that monocytes and macrophages undergo the greatest transcriptional changes (Figure 2F) in Gl261 tumor-bearing IFN$\alpha R^{-/-}$ mice. As expected, the absence of type I IFN signaling induced downregulation of ISGs (*Oas1g, Ifit3b, Oas1a, Ifit3, Ifi27L2a, Oas2, Ifit1bl1*), suggesting that a population of interferon-responsive myeloid cells were affected. On the other hand, genes primarily associated with M1 and M2 macrophage polarization (*Moxd1, Retnla, Rnase2a, Cd209e*) were upregulated in the absence of type I IFN signaling.[23–25] Altogether, these findings suggest that the absence of type I IFN signaling induced the greatest transcriptional changes among these tumor-infiltrating monocytes and macrophages.

Type I interferons regulate the polarization of tumor-infiltrating macrophages

Within the intratumoral myeloid compartment, tumor-associated macrophages (TAMs) constitute a heterogeneous cell population of the tumor microenvironment and acquire a broad spectrum of phenotypic, metabolic, and functional profiles in response to the specific tumor microenvironment.[26] In order to investigate the transcriptional changes that were induced as a result of IFNAR deficiency, we performed subclustering analysis into monocyte and macrophage populations. UMAP clustering analysis revealed a small population of monocytes

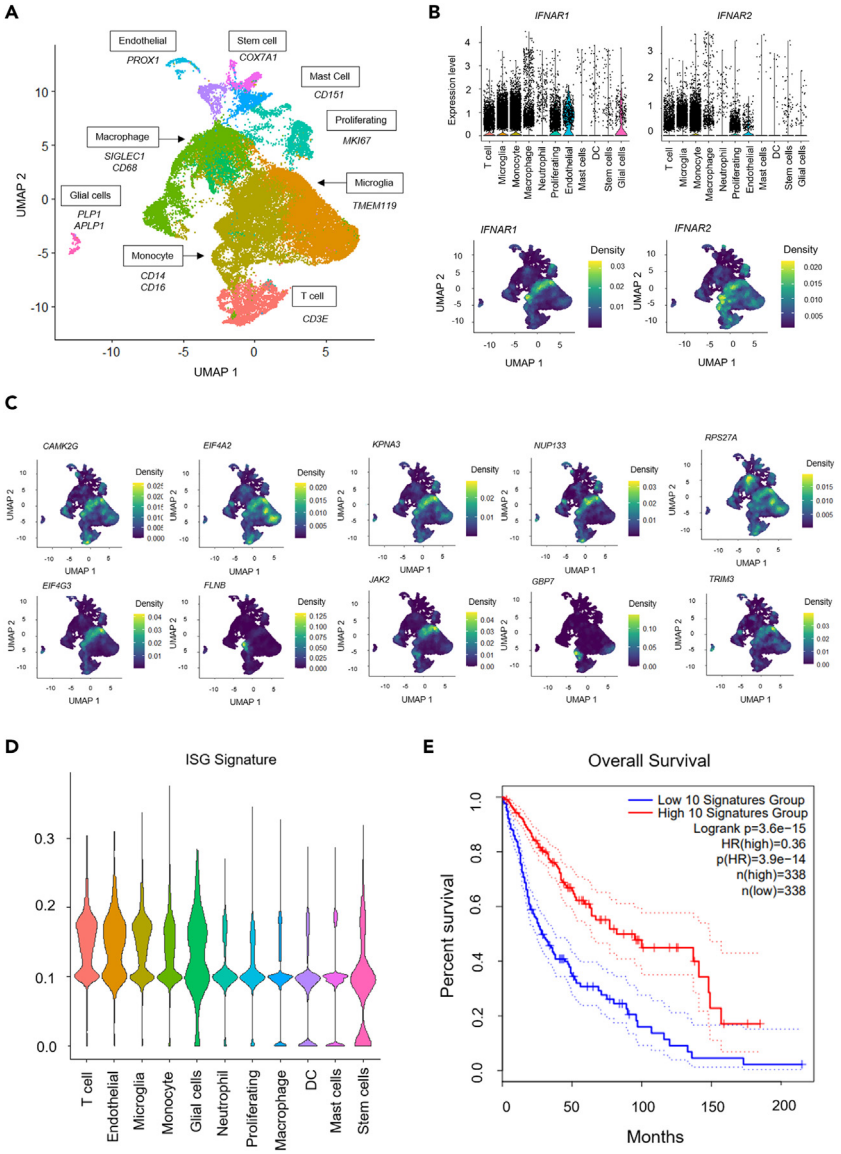

Figure 1. Immune landscape analysis of newly diagnosed GBM patient reveals ISG signature among tumor-infiltrating myeloid cells

(A) Uniform manifold approximation and projection (UMAP) plot showing the major tumor-infiltrating cells of newly diagnosed GBM patient clustered by their respective gene expressions.

(B) Violin plot comparing the expression of *IFNAR1* and *IFNAR2* among cell subsets of the immune landscape. Density plots also show the relative expression of *IFNAR1* and *IFNAR2*.

(C) Expression levels of interferon stimulated genes (*CAMK2G*, *EIF4A2*, *KPNA3*, *NUP133*, *RPS27A*, *EIF4G3*, *FLNB*, *JAK2*, *GBP7*, and *TRIM3*) shown through density plots.

(D) Violin plot showing comparing the levels of ISG signature score for immune cell subsets.

(E) Survival analysis using The Cancer Genome Atlas (TCGA) LGG and GBM dataset showing that a high expression of ISGs across myeloid cells correlated with increased patient survival.

(*Ace, F13a1*) and a heterogeneous population of TAMs: an interferon responsive cluster (*Ifi209, Ifi203, Ifi211*), a population of activated TAMs (*Ilr1b, Tlr2, Ilr1a*), proinflammatory (*Thbs1, Clec4e, Ilr1b*), anti-inflammatory (*Ccl24, Mrc1, Arg1*), complement activation associated TAMs (*C1qa, C1qb, C1qc*) (Figures 3A and 3B; Figure S3A). Gene set enrichment analysis (GSEA) showed the upregulation of gene sets related to fatty acid metabolism, oxidative phosphorylation, and adipogenesis in the absence of type I IFN signaling (Figure 3C). This is consistent with the notion that protumoral M2 TAMs employ oxidative metabolism and exhibit elevated fatty acid consumption.[27]

During macrophage polarization, M1 macrophages, otherwise known as classically activated macrophages, are characterized by a distinct chemokine repertoire. M1 polarization is accompanied by a production of CC chemokines and IFN-γ responsive chemokines that recruit

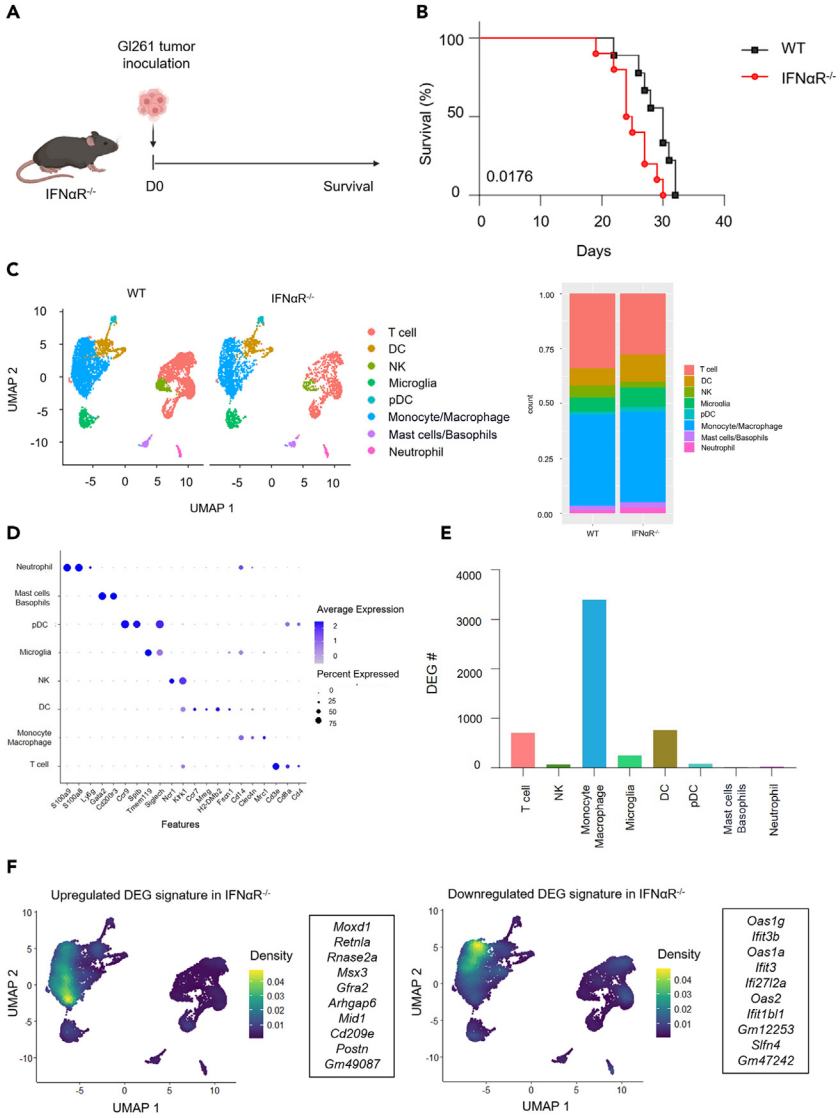

Figure 2. IFNAR deficiency induces transcriptional changes within the myeloid compartment of the GBM TME

(A) Experimental scheme for experiments using Wild type (WT) and IFNαR$^{-/-}$ mice intracranially injected with Gl261 cells (1×10^5) suspended in DPBS.

(B) Comparison of median survival of WT (30 days; $n = 9$) was compared with IFNαR$^{-/-}$mice (24.5 days; $n = 10$, $p = 0.0176$). Differences in survival were analyzed by Log rank (Mantel-Cox) test. The survival comparison results represent two or more independent experiments.

(C) UMAP analysis of tumor-infiltrating immune cells (left) and a barplot showing the frequencies of each immune cell subset between WT and IFNαR$^{-/-}$ mice (right).

(D) Dot plot showing the main features (*S100a9*, *S100a8*, *Ly6g*, *Gata2*, *Cd200r3*, *Ccr9*, *Spib*, *Tmem119*, *Siglech*, *Ncr1*, *Klrk1*, *Ccr7*, *Mreg*, *H2-Dmb2*, *Fscn1*, *Cd14*, *Clec4n*, *Mrc1*, *Cd3e*, *Cd8a*, and *Cd4*) to distinguish between neutrophils, mast cells & basophils, plasmacytoid dendritic cells, microglia, NK cells, dendritic cells, monocytes & macrophages, and T cells.

(E) Bar graph comparing the number of differentially expressed genes (DEGs) of each immune cell subset. Tumor-infiltrating monocytes and macrophages show the highest number of total DEGs.

(F) Differentially expressed genes (DEGs) were found using the FindMarkers function. DEG signature scores were assessed based on the top 15 upregulated and downregulated genes in IFNαR$^{-/-}$ mice. Top 10 of these top 15 upregulated and downregulated DEGs are indicated in the respective boxes to the right. Density plots show where these DEGs are primarily expressed.

helper T cells to coordinate a type I immune response, including CCL2, CCL3, CCL5, CXCL9, CXCL10, and CXCL16.[28] M2 macrophage polarization is accompanied by a distinct profile of transcriptionally activated genes, such as *Arg1*, *Mrc1*, *Chil3*, and *Ccl24*, that are induced as a result of tyrosine phosphorylation and activation of STAT6.[28–31] In addition, previous research has suggested the role of *Mid1* in potentiating macrophage protumoral functions.[32] When we compared the expression of some of these anti-inflammatory markers, we saw increased expression of *Arg1*, *Mrc1*, *Ccl24*, *Ear2*, *Chil3*, and *Mid1* among IFNAR deficient mice and a decrease in M1 proinflammatory markers *Ccl2*,

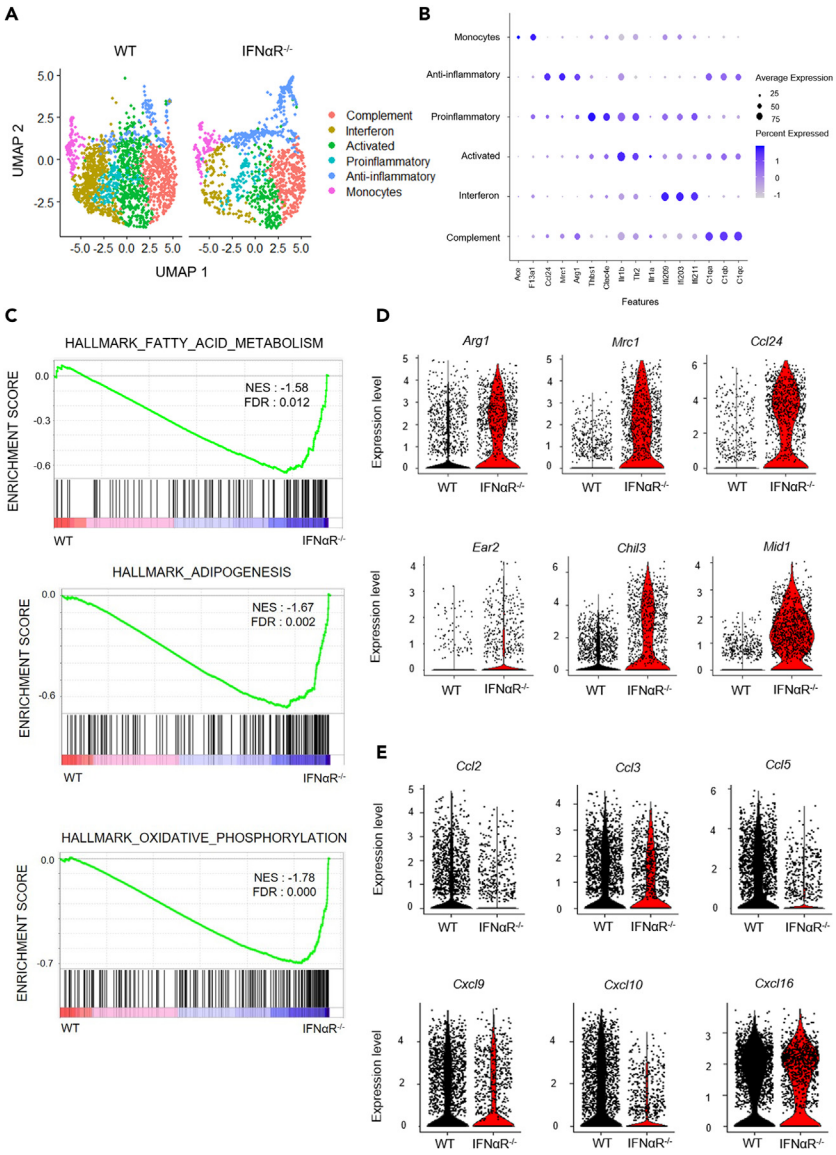

Figure 3. Absence of IFN signaling induces transcriptional changes of tumor-infiltrating monocytes and macrophages (TAMs)

(A) UMAP analysis of tumor-associated monocyte and macrophage subclusters.

(B) Dotplot showing the main features used to distinguish between monocytes (*Ace*, *F13a1*) TAM subclusters. TAMs were divided into anti-inflammatory (*Ccl24*, *Mrc1*, *Arg1*), proinflammatory (*Thbs1*, *Clec4e*), activated (*Il1rb*, *Tlr2*), interferon-responsive (*Ifi209*, *Ifi203*, *Ifi211*), and complement activation associated TAMs (*C1qa*, *C1qb*, *C1qc*).

(C) Gene set enrichment analysis (GSEA) using the DEGs of monocytes and macrophages in Gl261 tumor-bearing WT and IFNαR$^{-/-}$ mice.

(D) Violin plots comparing the expression of anti-inflammatory markers *Arg1*, *Mrc1*, *Ccl24*, *Ear2*, *Chil3*, and *Mid1* between tumor-bearing WT and IFNαR$^{-/-}$ mice.

(E) Violin plots comparing the expression of proinflammatory markers *Ccl2*, *Ccl3*, *Ccl5*, *Cxcl9*, *Cxcl10*, and *Cxcl16* between tumor-bearing WT and IFNαR$^{-/-}$ mice.

Ccl3, *Ccl5*, *Cxcl9*, *Cxcl10*, and *Cxcl16* (Figures 3D and 3E; Figure S3C). We were able to predict that the absence of type I IFNs promotes the polarization of the macrophage compartment into a state that favors tumor progression.

In addition to the polarization of anti-inflammatory macrophages, we found an increase in TAMs expressing complement activation mediators *C1qa*, *C1qb*, and *C1qc* in the absence of type I IFN signaling (Figures S3A and S3B). While the complement system has traditionally been considered an important part of immunosurveillance, it is also known to be involved in promoting tumor progression.[33,34] C1q is an important mediator of the complement cascade system and is predicted to affect macrophage metabolism toward an immunosuppressive phenotype by downregulating proinflammatory cytokine production.[35] There are findings that suggest an association between C1q^{+} macrophages and T cell exhaustion by inhibiting CD8^{+} T cell activation, proliferation, and cytotoxic functions.[36] These complement TAMs increased in the absence of type I IFN signaling, allowing us to question its impact on the T cell lymphoid compartment of the GBM TME.

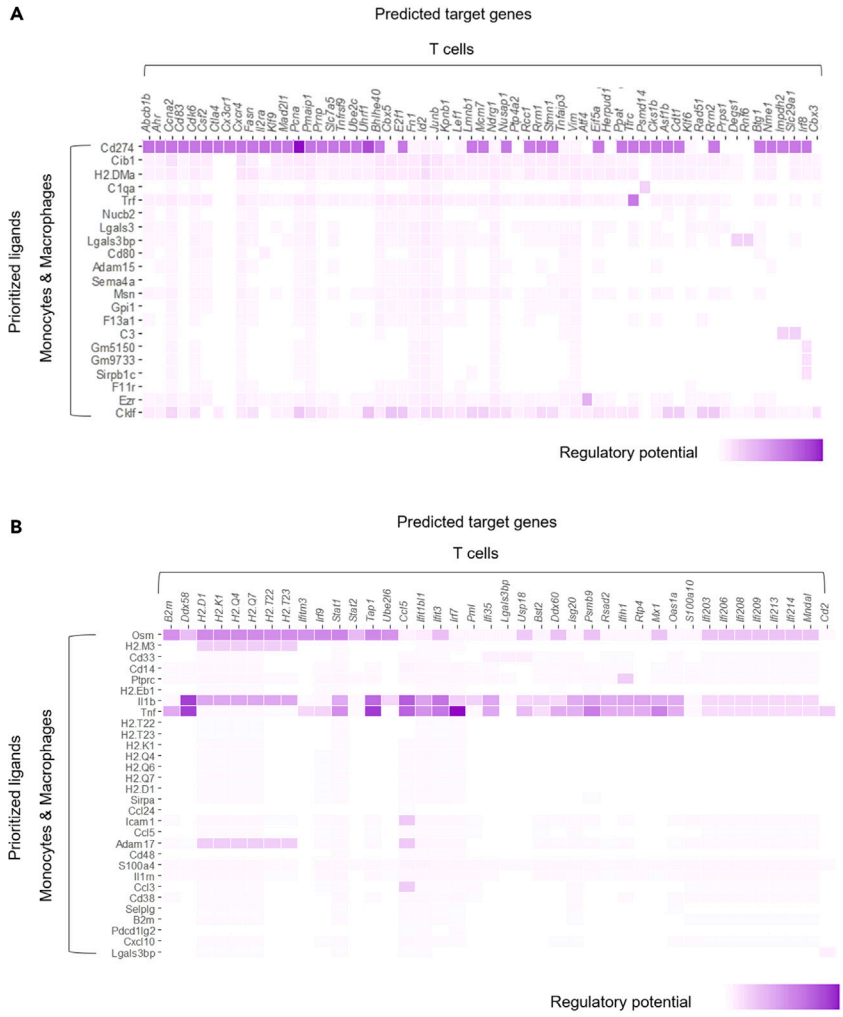

Figure 4. Lack of proper type I IFN production enhances interactions between PD-L1 and its target genes

(A) Heatmap showing the upregulated interactions between tumor-infiltrating myeloid cells and T cells in tumor-bearing IFNαR$^{-/-}$ mice. Y axis represents the expression of prioritized ligands from tumor-infiltrating monocytes and macrophages. X axis represents the target gene expression induced in T cells by the respective ligand.

(B) Heatmap showing the downregulated interactions between tumor-infiltrating myeloid cells and T cells in tumor-bearing WT mice. Y axis represents the expression of prioritized ligands from tumor-infiltrating monocytes and macrophages. X axis represents the target gene expression induced in T cells by the respective ligand.

Absence of type I interferon signaling enhances the PD-L1 pathway between tumor-associated macrophages and T cells in the tumor microenvironment

In order to investigate how type I IFNs play a role in mediating the interaction between TAMs and T cells, we wanted to see how gene expression changes in T cells induced by type I IFN absence were influenced by intratumoral macrophages. We applied NicheNet analysis to the immune cells of the GBM TME with monocytes & macrophages as the "sender" and T cells as the "receiver" to study the intercellular communication networks between these cell types.[37] Based on the DEGs that were upregulated in the absence of type I IFN signaling, we were able to see that *Cd274,* which encodes for PD-L1, most likely regulated the expression of many genes among T cells (Figure 4A). We were able to predict that the absence of type I IFNs enhances interactions between PD-L1 expressing intratumoral myeloid cells and T cells. On the other hand, based on the DEGs that were upregulated in WT mice, we were able to see that gene expression among T cells was most likely affected by the prioritized ligands *Il1b* and *Tnf* (Figure 4B). M1 macrophages are characterized by the expression of TNF-α and Il-1β and coordinate a type I immune response suited for intracellular pathogen killing and tumor resistance.[28,38] Thus, we were able to predict that the proper production of type I IFNs polarized a population of macrophages to acquire an antitumoral phenotype, including *Il1b* and *Tnf* expressing macrophages. Most of the genes that were induced in T cells were interferon-stimulated genes, suggesting that interactions between *Il1b* and *Tnf*-expressing macrophages affected a population of interferon-responsive T cells. As

suggested by previous research, interferon-responsive T cells are likely to have enhanced effector function, activation, and prolonged survival which potentiate cancer immunosurveillance.[39–42]

Enhanced PD-L1 interactions induced by the absence of type I interferon signaling affect T cell functionality

Subclustering analysis into T cells revealed distinct populations of CD8 T cells and further characterization of CD8 T cells showed cell populations that were interferon-responsive (*Stat1, Ifi209, Ifi206*) and cell-cycle related (*Cdca7, Cdc6, Stmn1*), along with a small population of proliferating (*Mki67*), effector (*Gzmf, Gzmc, Gzmb*), and cells that expressed NK receptors and proteins (*Klra1, Klra7, Klra6*) (Figure 5A). We found decreased infiltration of CD8 T cells to the TME (Figure S4B) and UMAP comparison of CD8 T cell subclusters showed decreases in effector and interferon-responsive CD8 T cell subclusters (Figure 5B), which was consistent with GSEA pathway analysis. GSEA analysis showed enrichment in gene sets related to TCR signaling, and regulation of T cell-mediated cytotoxicity (Figure 5C), suggesting that the absence of type I IFNs perturbs these respective pathways. Functional analysis of T cells was performed from brain tumor tissues 20 days following GI261 implantation. To confirm that the absence of type I IFN signaling reduces T cell cytotoxicity, CD8 T cells were analyzed for cytokine expression. We found decreased expression of IFN-γ and TNF-α, as well as granulation markers CD107a and Granzyme B (Figures 5D and 5E). Analysis of T cell coinhibitory marker expression revealed increased CD244 (2B4) among CD8 T cells in the absence of type I IFN signaling and slight increases in PD-1 expression as well (Figure 5F; Figures S4A and S4D). In addition to CD8 T cells, we found decreased cytotoxicity among CD4 T cells as well (Figure S4C). Altogether, we were able to see that CD8 T cell functional responses were dampened in the absence of type I IFN signaling and that this may be a result of enhanced PD-L1 interactions among tumor-infiltrating macrophages.

Anti-PD1 treatment enhances CXCR6^{+} CD8 T cell infiltration

One of the main successful trials in cancer immunotherapy has been associated with PD-1/PD-L1 blocking therapy.[43] A major factor that predicts responsiveness to immune checkpoint blockade therapy is type I IFNs. Past studies have confirmed that patient overall survival following checkpoint blockade is enhanced in tumors that have high type I IFN signaling.[44] In order to assess if the immunosuppressive myeloid compartment induced through the absence of type I IFN signaling could be transcriptionally reprogrammed through checkpoint inhibitors, we treated IFNαR$^{-/-}$ mice with anti-PD1 and performed scRNA-seq on CD45.2^{+} immune cells (Figure 6A). UMAP analysis showed distinct immune cell populations (Figure 6B). In order to gain an overview of intercellular signaling networks between cell types, we conducted CellChat analysis and saw that monocytes and macrophages participated in sending outgoing signals involved in the CXCL signaling network (Figures S5A and S5B). T cells received nearly all outgoing signals associated with the CXCL signaling network (Figure 6C). Further analysis revealed interactions between CXCL16^{+} monocytes & macrophages and CXCR6^{+} T cells (Figure S5C). There is evidence that CXCL16 and its receptor CXCR6 are positively correlated with T cell infiltration, and this CXCL16/CXCR6 axis plays a critical role in generating antitumor immunity. We first confirmed the expression of *Cxcl6* among tumor-infiltrating monocyte and macrophage populations and also confirmed that *Cxcr6* was exclusively expressed among lymphoid T cell populations (Figure 6D). We saw that CD8 T cell infiltration increased in anti-PD1 treated IFNαR$^{-/-}$ mice (Figure 6E). These CD8 T cells showed increased levels of *Cxcr6* in anti-PD1 treated IFNαR$^{-/-}$ mice (Figure 6F and Figure S5D), suggesting an increase in *Cxcr6*$^{+}$ CD8 T cell infiltration into the TME following anti-PD1 treatment.

Functional analysis of CD8 T cells of anti-PD1 treated IFNαR$^{-/-}$ mice showed no significant difference in cytokine expression of IFN-γ and TNF-α and no significant difference in expression of T cell coinhibitory markers 2B4 and TIM-3 (Figure S5E). This indicates that treatment with anti-PD1 may have restored CD8 T cell functionality. Altogether, we were able to see that even in the absence of proper type I IFN production, administration of anti-PD1 can enhance CXCR6^{+} CD8 T cell infiltration which may contribute to at least restoring T cell cytokine production and narrowing the survival difference than what was initially observed (Figure S5F).

DISCUSSION

By using various single-cell RNA sequencing techniques, we analyzed changes in the GBM immune landscape in the lack of proper type I IFN signaling, with a specific focus on tumor-infiltrating myeloid cells. Our results show that type I IFNs play an important role in regulating the crosstalk between tumor-infiltrating myeloid cells and T cells in the GBM TME by inducing transcriptional changes favoring tumor progression. In the lack of proper type I IFN production, tumor-infiltrating macrophages undergo transcriptional changes that consist of upregulation in metabolic processes related to lipid metabolism and increased anti-inflammatory signature, which is consistent with the notion that protumoral TAMs are characterized by increased fatty acid uptake and accumulation in the form of lipid droplets.[45] We predict that the absence of type I IFN signaling may also affect the spatial organization of tumor-associated macrophage subsets. Spatial transcriptomic analysis of human glioma samples showed the localization of IFN-responsive macrophages and macrophages enriched in lipid metabolism. Both of these macrophage clusters are localized in the perivascular regions as opposed to the necrotic regions of the GBM tumor.[46] The different localizations of macrophage clusters may correlate with their antitumoral or protumoral functions and also reflect the metabolic state of the tumor microenvironment.[31] It will be helpful to investigate how the localization of tumor-associated macrophages is affected when the type I IFN signaling axis is perturbed. Future studies will explore the spatial patterning of TAM subsets in GBM patient samples.

While previous studies have shown that type I IFNs induce expression of PD-L1 and PD-1 in myeloid cells, our study here hypothesizes that the absence of type I IFN signaling strengthens interactions between PD-L1 and its target genes.[44] Further analysis investigating the involvement of strengthened PD-L1 interactions in anti-tumor immunity suggests that lymphoid cells may be affected as well. We see that CD8 T cells

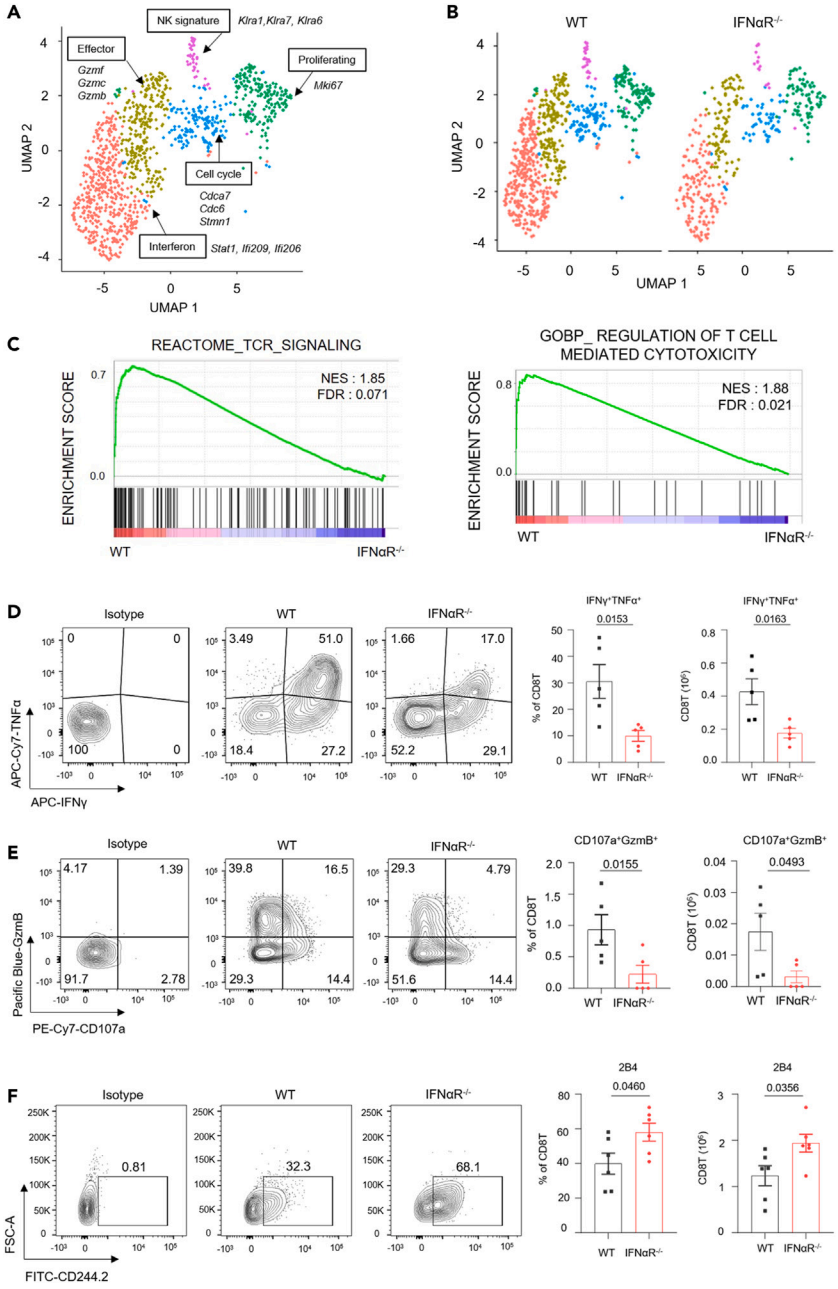

Figure 5. CD8 T cell functional responses are dampened by the lack of proper IFN signaling

(A) UMAP analysis of CD8 T cell subclusters: effector (*Gzmf*, *Gzmc*, and *Gzmb*), interferon-responsive (*Stat1*, *Ifi209*, and *Ifi206*), cell-cycle related (*Cdca7*, *Cdc6*, and *Stmn1*), proliferating (*Mki67*), and cells with NK signature (*Klra1*, *Klra7*, and *Klra6*).

(B) UMAP analysis comparing CD8 T cell subclusters between tumor-bearing WT and IFNαR$^{-/-}$ mice.

(C) GSEA analysis using the DEGs of CD8 T cells expressed in WT and IFNαR$^{-/-}$ mice.

(D) Representative flow cytometry plots for IFN-γ and TNF-α expression from CD8 T cells of WT and IFNαR$^{-/-}$ mice (left). Bar graphs depict the frequencies and numbers of IFN-γ and TNF-α expressed as percentages among CD8 T cells (right). The data represent the mean ± standard error of the mean. FACS data represent two or more independent experiments.

(E) Representative flow cytometry plots for CD107a and Granzyme B expression from CD8 T cells of WT and IFNαR$^{-/-}$ mice (left). Bar graphs depict the frequencies and numbers of CD107a and Granzyme B expressed as percentages among CD8 T cells (right). The data represent the mean ± standard error of the mean. FACS data represent two or more independent experiments.

(F) Representative flow cytometry plots for 2B4 expression from CD8 T cells of WT and IFNαR$^{-/-}$ mice (left). Bar graphs depicting the frequencies and number of 2B4 among CD8 T cells in WT and IFNαR$^{-/-}$ mice (right). The data represent the mean ± standard error of the mean. FACS data represent two or more independent experiments. The data were analyzed by two-tailed unpaired Student's t test (5D-5F).

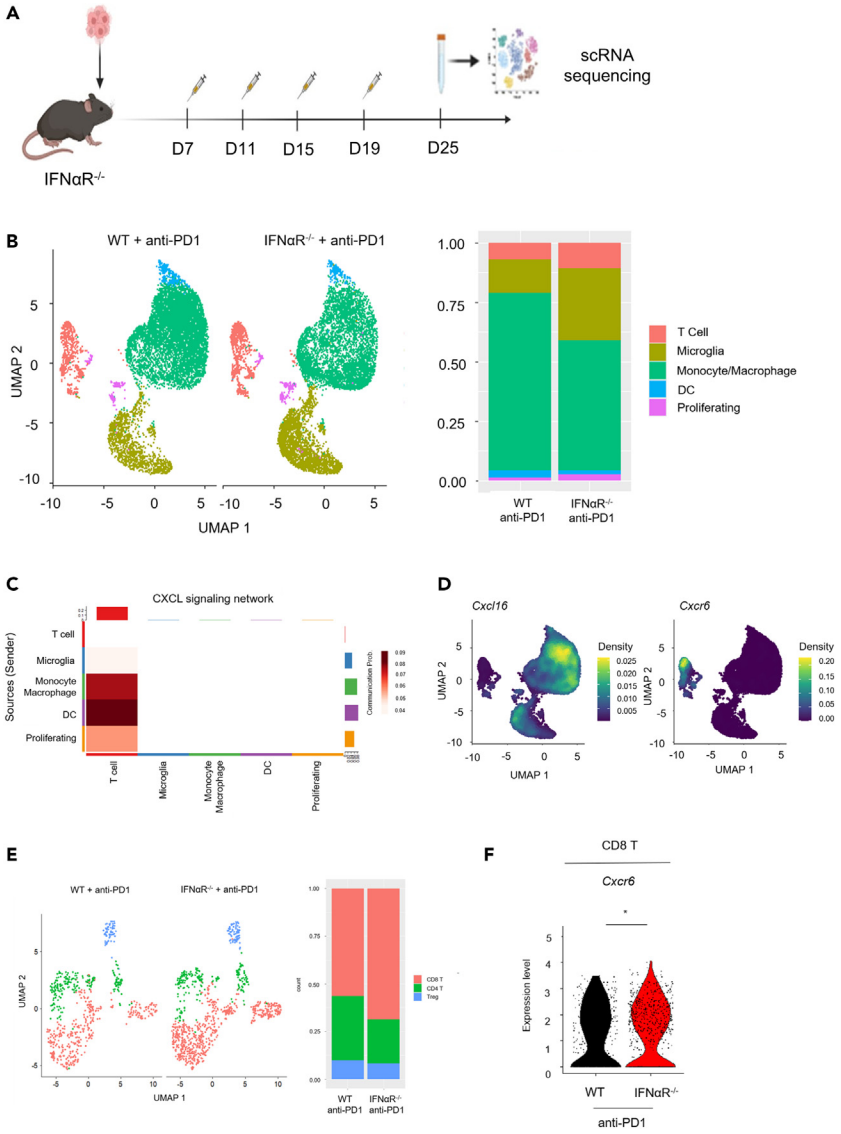

Figure 6. Anti-PD1 treatment enhances CXCR6^{+} CD8 T cell infiltration in tumor-bearing IFNαR$^{-/-}$ mice

(A) Experimental scheme for experiments to determine the changes in immune cell populations of anti-PD1 treated Gl261 tumor-bearing WT and IFNαR$^{-/-}$mice. Anti-PD1 was intraperitoneally injected at a dose of 200 μg per mouse on days 7, 11, 15, and 19 after tumor injection (D0). Immune cells were harvested and sorted on 25 days following tumor injection (D25).

(B) UMAP analysis comparing immune cell infiltrates of anti-PD1 treated tumor-bearing WT and IFNαR$^{-/-}$ mice (left) and a barplot showing the frequencies of each immune cell subset between anti-PD1 treated WT and IFNαR$^{-/-}$ mice (right).

(C) Heatmap shows the cells that send outgoing signals involved in the CXCL signaling network and the cells that are receiving these outgoing signals.

(D) Density plot shows the expression of *Cxcl16* among tumor-infiltrating monocytes and macrophages and *Cxcr6* almost exclusively expressed in T cells.

(E) UMAP analysis compares T cell subset infiltration of anti-PD1 treated tumor-bearing WT and IFNαR$^{-/-}$ mice (left). Barplot compares the frequencies of CD4 T cell, regulatory T cell, and CD8 T cell infiltration of anti-PD1 treated tumor-bearing WT and IFNαR$^{-/-}$ mice (right).

(F) Violin plot comparison shows levels of *Cxcr6* expression in CD8 T cells between anti-PD1 treated tumor-bearing WT and IFNαR$^{-/-}$ mice. Data were analyzed by the stat_compare_means function with an unpaired *t*-test. *$p < 0.05$.

produced decreased levels of effector molecules, suggesting that increased PD-L1 interactions between TAMs and CD8 T cells dampened anti-tumor immune responses.

More importantly, we see that treatment with anti-PD1 can at least alleviate some of the immunosuppression derived from the lack of type I IFN signaling. Anti-PD1 treatment reprograms the myeloid compartment into one that disfavors tumor progression by suppressing PD-L1 interactions and increasing CXCR6^{+} CD8 T cell infiltration, which is known to be important for intratumoral CD8 T cell efficacy.[47] We see that anti-PD1 treatment at least contributes to the recovery of CD8 T cell functions, yet there is still insufficient evidence to say that immune

checkpoint blockade therapy is enough to rescue or reinvigorate CD8 T cell function in the absence of type I IFN signaling because further screening of CD8 T cell functional and inhibitory marker expression is needed. Further study is needed to confirm that the administration of anti-PD1 is enough to compensate for the lack of type I IFN production.

Limitations of the study

In conclusion, we demonstrate here that type I IFN production is crucial in eliciting anti-tumor immune responses against GBM. The results of our study, however, have some drawbacks. There is still much to learn about how type I IFNs regulate myeloid and lymphoid cell dynamics in the GBM TME. Although we demonstrated that tumor-infiltrating monocytes and macrophages are driven to a protumoral state in the absence of type I IFN signaling, how these cells interact with other innate lymphoid cells still needs further investigation. A comprehensive functional analysis of IFNAR-deficient tumor-infiltrating myeloid cells following anti-PD1 treatment is needed to gain a better understanding of immune cell dynamics.

RESOURCE AVAILABILITY

Lead contact

Requests for resources, reagents, and further information should be directed to the lead contact, Heung Kyu Lee (heungkyu.lee@kaist.ac.kr).

Materials availability

All mouse lines and materials used in this study were provided or purchased from mentioned companies or researchers. This study did not generate any new or unique reagents.

Data and code availability

- Single-cell RNA-seq data have been deposited and are available under accession code GSE264251 in Gene Expression Omnibus (GEO) at the National Center for Biotechnology Information (NCBI).
- This article does not report the original code.
- Any additional information required to reanalyze the data reported in this article is available from the lead contact upon request.

ACKNOWLEDGMENTS

The authors thank Ji Ye Kim at the Biomedical Research Center for technical service and all members of the Laboratory of Host Defenses for helpful discussion. This work was supported by the National Research Foundation of Korea grant (NRF-2021M3A9D3026428, NRF-2023R1A2C3003825, and RS-2024-00439735). This study was also supported by the Samsung Science and Technology Foundation (SSTF-BA1902-05), Republic of Korea. Graphical abstract, Figure 6A and Figure S2A were created with BioRender.com.

AUTHOR CONTRIBUTIONS

J.L., J.L., H.C.K., I.K., B.H.K., K.B.K., Y.K., M.S.K., and H.K.L. designed and performed the experiments. J.L. and H.K.L. conceived the study, analyzed the data, and wrote the article. H.K.L supervised the study.

DECLARATION OF INTERESTS

The authors declare no competing interests.

STAR★METHODS

Detailed methods are provided in the online version of this paper and include the following:

- KEY RESOURCES TABLE
- EXPERIMENTAL MODEL AND STUDY PARTICIPANT DETAILS
  - Mice
  - Tumor cell lines
- METHOD DETAILS
  - Syngeneic mouse glioblastoma model
  - Analysis of human GBM patient data
  - Tumor digestion and single cell isolation
- QUANTIFICATION AND STATISTICAL ANALYSIS
  - Flow cytometry
  - Single-cell RNA sequencing
  - NicheNet analysis
  - CellChat analysis
  - Immune checkpoint blockade administration

SUPPLEMENTAL INFORMATION

Supplemental information can be found online at https://doi.org/10.1016/j.isci.2024.110810.

Received: April 8, 2024
Revised: August 2, 2024
Accepted: August 21, 2024

REFERENCES

1. Lim, M., Xia, Y., Bettegowda, C., and Weller, M. (2018). Current state of immunotherapy for glioblastoma. Nat. Rev. Clin. Oncol. *15*, 422–442. https://doi.org/10.1038/s41571-018-0003-5.
2. Kreatsoulas, D., Bolyard, C., Wu, B.X., Cam, H., Giglio, P., and Li, Z. (2022). Translational landscape of glioblastoma immunotherapy for physicians: guiding clinical practice with basic scientific evidence. J. Hematol. Oncol. *15*, 80. https://doi.org/10.1186/s13045-022-01298-0.
3. Patel, A.P., Tirosh, I., Trombetta, J.J., Shalek, A.K., Gillespie, S.M., Wakimoto, H., Cahill, D.P., Nahed, B.V., Curry, W.T., Martuza, R.L., et al. (2014). Single-cell RNA-seq highlights intratumoral heterogeneity in primary glioblastoma. Science *344*, 1396–1401. https://doi.org/10.1126/science.1254257.
4. Birocchi, F., Cusimano, M., Rossari, F., Beretta, S., Rancoita, P.M.V., Ranghetti, A., Colombo, S., Costa, B., Angel, P., Sanvito, F., et al. (2022). Targeted inducible delivery of immunoactivating cytokines reprograms glioblastoma microenvironment and inhibits growth in mouse models. Sci. Transl. Med. *14*, eabl4106. https://doi.org/10.1126/scitranslmed.abl4106.
5. Kao, K.C., Jaccard, A., and Ho, P.C. (2022). IFNalpha Potentiates Immune-Checkpoint Blockade by Rewiring Metabolic Cross-talk. Cancer Discov. *12*, 1615–1616. https://doi.org/10.1158/2159-8290.CD-22-0472.
6. Musella, M., Manic, G., De Maria, R., Vitale, I., and Sistigu, A. (2017). Type-I-interferons in infection and cancer: Unanticipated dynamics with therapeutic implications. OncoImmunology *6*, e1314424. https://doi.org/10.1080/2162402X.2017.1314424.
7. Zitvogel, L., Galluzzi, L., Kepp, O., Smyth, M.J., and Kroemer, G. (2015). Type I interferons in anticancer immunity. Nat. Rev. Immunol. *15*, 405–414. https://doi.org/10.1038/nri3845.
8. Gessani, S., and Belardelli, F. (2021). Type I Interferons as Joint Regulators of Tumor Growth and Obesity. Cancers *13*, 196. https://doi.org/10.3390/cancers13020196.
9. Peterson, C., Denlinger, N., and Yang, Y. (2022). Recent Advances and Challenges in Cancer Immunotherapy. Cancers *14*, 3972. https://doi.org/10.3390/cancers14163972.
10. Wei, S.C., Duffy, C.R., and Allison, J.P. (2018). Fundamental Mechanisms of Immune Checkpoint Blockade Therapy. Cancer Discov. *8*, 1069–1086. https://doi.org/10.1158/2159-8290.CD-18-0367.
11. Zemek, R.M., Chin, W.L., Fear, V.S., Wylie, B., Casey, T.H., Forbes, C., Tilsed, C.M., Boon, L., Guo, B.B., Bosco, A., et al. (2022). Temporally restricted activation of IFNbeta signaling underlies response to immune checkpoint therapy in mice. Nat. Commun. *13*, 4895. https://doi.org/10.1038/s41467-022-32567-8.
12. Keenan, T.E., Burke, K.P., and Van Allen, E.M. (2019). Genomic correlates of response to immune checkpoint blockade. Nat. Med. *25*, 389–402. https://doi.org/10.1038/s41591-019-0382-x.
13. Chen, P.L., Roh, W., Reuben, A., Cooper, Z.A., Spencer, C.N., Prieto, P.A., Miller, J.P., Bassett, R.L., Gopalakrishnan, V., Wani, K., et al. (2016). Analysis of Immune Signatures in Longitudinal Tumor Samples Yields Insight into Biomarkers of Response and Mechanisms of Resistance to Immune Checkpoint Blockade. Cancer Discov. *6*, 827–837. https://doi.org/10.1158/2159-8290.CD-15-1545.
14. Jacquelot, N., Yamazaki, T., Roberti, M.P., Duong, C.P.M., Andrews, M.C., Verlingue, L., Ferrere, G., Becharef, S., Vétizou, M., Daillère, R., et al. (2019). Sustained Type I interferon signaling as a mechanism of resistance to PD-1 blockade. Cell Res. *29*, 846–861. https://doi.org/10.1038/s41422-019-0224-x.
15. Gong, W., Donnelly, C.R., Heath, B.R., Bellile, E., Donnelly, L.A., Taner, H.F., Broses, L., Brenner, J.C., Chinn, S.B., Ji, R.R., et al. (2021). Cancer-specific type-I interferon receptor signaling promotes cancer stemness and effector CD8+ T-cell exhaustion. OncoImmunology *10*, 1997385. https://doi.org/10.1080/2162402X.2021.1997385.
16. Abdelfattah, N., Kumar, P., Wang, C., Leu, J.-S., Flynn, W. F., Gao, R., Baskin, D. S., Pichumani, K., Ijare, O. B., Wood, S. L., et al. (2022). Single-cell analysis of human glioma and immune cells identifies S100A4 as an immunotherapy target. Nat. Commun. *13*, 767. https://doi.org/10.1038/s41467-022-28372-y.
17. Platanias, L.C. (2005). Mechanisms of type-I- and type-II-interferon-mediated signalling. Nat. Rev. Immunol. *5*, 375–386. https://doi.org/10.1038/nri1604.
18. Minn, A.J. (2015). Interferons and the Immunogenic Effects of Cancer Therapy. Trends Immunol. *36*, 725–737. https://doi.org/10.1016/j.it.2015.09.007.
19. Hubel, P., Urban, C., Bergant, V., Schneider, W.M., Knauer, B., Stukalov, A., Scaturro, P., Mann, A., Brunotte, L., Hoffmann, H.H., et al. (2019). A protein-interaction network of interferon-stimulated genes extends the innate immune system landscape. Nat. Immunol. *20*, 493–502. https://doi.org/10.1038/s41590-019-0323-3.
20. Singh, D.K., Aladyeva, E., Das, S., Singh, B., Esaulova, E., Swain, A., Ahmed, M., Cole, J., Moodley, C., Mehra, S., et al. (2022). Myeloid cell interferon responses correlate with clearance of SARS-CoV-2. Nat. Commun. *13*, 679. https://doi.org/10.1038/s41467-022-28315-7.
21. Lamot, L., Niemietz, I., and Brown, K.L. (2019). Methods for type I interferon detection and their relevance for clinical utility and improved understanding of rheumatic diseases. Clin. Exp. Rheumatol. *37*, 1077–1083.
22. Taniguchi, T., and Takaoka, A. (2001). A weak signal for strong responses: interferon-alpha/beta revisited. Nat. Rev. Mol. Cell Biol. *2*, 378–386. https://doi.org/10.1038/35073080.
23. Wang, S., Wang, J., Chen, Z., Luo, J., Guo, W., Sun, L., and Lin, L. (2024). Targeting M2-like tumor-associated macrophages is a potential therapeutic approach to overcome antitumor drug resistance. npj Precis. Oncol. *8*, 31. https://doi.org/10.1038/s41698-024-00522-z.
24. Geeraerts, X., Fernández-Garcia, J., Hartmann, F.J., de Goede, K.E., Martens, L., Elkrim, Y., Debraekeleer, A., Stijlemans, B., Vandekeere, A., Rinaldi, G., et al. (2021). Macrophages are metabolically heterogeneous within the tumor microenvironment. Cell Rep. *37*, 110171. https://doi.org/10.1016/j.celrep.2021.110171.
25. Pombo Antunes, A.R., Scheyltjens, I., Lodi, F., Messiaen, J., Antoranz, A., Duerinck, J., Kancheva, D., Martens, L., De Vlaminck, K., Van Hove, H., et al. (2021). Single-cell profiling of myeloid cells in glioblastoma across species and disease stage reveals macrophage competition and specialization. Nat. Neurosci. *24*, 595–610. https://doi.org/10.1038/s41593-020-00789-y.
26. Puthenveetil, A., and Dubey, S. (2020). Metabolic reprograming of tumor-associated macrophages. Ann. Transl. Med. *8*, 1030. https://doi.org/10.21037/atm-20-2037.
27. Zhang, S., Lv, K., Liu, Z., Zhao, R., and Li, F. (2024). Fatty acid metabolism of immune cells: a new target of tumour immunotherapy. Cell Death Dis. *10*, 39. https://doi.org/10.1038/s41420-024-01807-9.
28. Mantovani, A., Sica, A., Sozzani, S., Allavena, P., Vecchi, A., and Locati, M. (2004). The chemokine system in diverse forms of macrophage activation and polarization. Trends Immunol. *25*, 677–686. https://doi.org/10.1016/j.it.2004.09.015.
29. Yu, T., Gan, S., Zhu, Q., Dai, D., Li, N., Wang, H., Chen, X., Hou, D., Wang, Y., Pan, Q., et al. (2019). Modulation of M2 macrophage polarization by the crosstalk between Stat6 and Trim24. Nat. Commun. *10*, 4353. https://doi.org/10.1038/s41467-019-12384-2.
30. Chen, J., Huang, X.R., Yang, F., Yiu, W.H., Yu, X., Tang, S.C.W., and Lan, H.Y. (2022). Single-cell RNA Sequencing Identified Novel Nr4a1+ Ear2+ Anti-Inflammatory Macrophage Phenotype under Myeloid-TLR4 Dependent Regulation in Anti-Glomerular Basement Membrane (GBM) Crescentic Glomerulonephritis (cGN). Adv. Sci. *9*, 2200668. https://doi.org/10.1002/advs.202200668.
31. Sattiraju, A., Kang, S., Giotti, B., Chen, Z., Marallano, V.J., Brusco, C., Ramakrishnan, A., Shen, L., Tsankov, A.M., Hambardzumyan, D., et al. (2023). Hypoxic niches attract and sequester tumor-associated macrophages and cytotoxic T cells and reprogram them for immunosuppression. Immunity *56*, 1825–1843.e6. https://doi.org/10.1016/j.immuni.2023.06.017.
32. Fang, M., Zhang, A., Du, Y., Lu, W., Wang, J., Minze, L.J., Cox, T.C., Li, X.C., Xing, J., and Zhang, Z. (2022). TRIM18 is a critical regulator of viral myocarditis and organ inflammation. J. Biomed. Sci. *29*, 55. https://doi.org/10.1186/s12929-022-00840-z.
33. Mantovani, A., Allavena, P., Marchesi, F., and Garlanda, C. (2022). Macrophages as tools and targets in cancer therapy. Nat. Rev. Drug Discov. *21*, 799–820. https://doi.org/10.1038/s41573-022-00520-5.
34. Senent, Y., Tavira, B., Pio, R., and Ajona, D. (2022). The complement system as a

regulator of tumor-promoting activities mediated by myeloid-derived suppressor cells. Cancer Lett. *549*, 215900. https://doi.org/10.1016/j.canlet.2022.215900.

35. Spivia, W., Magno, P.S., Le, P., and Fraser, D.A. (2014). Complement protein C1q promotes macrophage anti-inflammatory M2-like polarization during the clearance of atherogenic lipoproteins. Inflamm. Res. *63*, 885–893. https://doi.org/10.1007/s00011-014-0762-0.
36. Roumenina, L.T., Daugan, M.V., Noé, R., Petitprez, F., Vano, Y.A., Sanchez-Salas, R., Becht, E., Meilleroux, J., Clec'h, B.L., Giraldo, N.A., et al. (2019). Tumor Cells Hijack Macrophage-Produced Complement C1q to Promote Tumor Growth. Cancer Immunol. Res. *7*, 1091–1105. https://doi.org/10.1158/2326-6066.CIR-18-0891.
37. Browaeys, R., Saelens, W., and Saeys, Y. (2020). NicheNet: modeling intercellular communication by linking ligands to target genes. Nat. Methods *17*, 159–162. https://doi.org/10.1038/s41592-019-0667-5.
38. Murray, P.J., Allen, J.E., Biswas, S.K., Fisher, E.A., Gilroy, D.W., Goerdt, S., Gordon, S., Hamilton, J.A., Ivashkiv, L.B., Lawrence, T., et al. (2014). Macrophage activation and polarization: nomenclature and experimental guidelines. Immunity *41*, 14–20. https://doi.org/10.1016/j.immuni.2014.06.008.
39. Le Bon, A., Durand, V., Kamphuis, E., Thompson, C., Bulfone-Paus, S., Rossmann, C., Kalinke, U., and Tough, D.F. (2006). Direct Stimulation of T Cells by Type I IFN Enhances the CD8+ T Cell Response during Cross-Priming1. J. Immunol. *176*, 4682–4689. https://doi.org/10.4049/jimmunol.176.8.4682.
40. Curtsinger, J.M., Valenzuela, J.O., Agarwal, P., Lins, D., and Mescher, M.F. (2005). Cutting Edge: Type I IFNs Provide a Third Signal to CD8 T Cells to Stimulate Clonal Expansion and Differentiation1. J. Immunol. *174*, 4465–4469. https://doi.org/10.4049/jimmunol.174.8.4465.
41. Kolumam, G.A., Thomas, S., Thompson, L.J., Sprent, J., and Murali-Krishna, K. (2005). Type I interferons act directly on CD8 T cells to allow clonal expansion and memory formation in response to viral infection. J. Exp. Med. *202*, 637–650. https://doi.org/10.1084/jem.20050821.
42. Lu, C., Klement, J.D., Ibrahim, M.L., Xiao, W., Redd, P.S., Nayak-Kapoor, A., Zhou, G., and Liu, K. (2019). Type I interferon suppresses tumor growth through activating the STAT3-granzyme B pathway in tumor-infiltrating cytotoxic T lymphocytes. J. Immunother. Cancer *7*, 157. https://doi.org/10.1186/s40425-019-0635-8.
43. Jia, L., Zhang, Q., and Zhang, R. (2018). PD-1/PD-L1 pathway blockade works as an effective and practical therapy for cancer immunotherapy. Cancer Biol. Med. *15*, 116–123. https://doi.org/10.20892/j.issn.2095-3941.2017.0086.
44. Klement, J.D., Redd, P.S., Lu, C., Merting, A.D., Poschel, D.B., Yang, D., Savage, N.M., Zhou, G., Munn, D.H., Fallon, P.G., and Liu, K. (2023). Tumor PD-L1 engages myeloid PD-1 to suppress type I interferon to impair cytotoxic T lymphocyte recruitment. Cancer Cell *41*, 620–636.e9. https://doi.org/10.1016/j.ccell.2023.02.005.
45. Shao, N., Qiu, H., Liu, J., Xiao, D., Zhao, J., Chen, C., Wan, J., Guo, M., Liang, G., Zhao, X., and Xu, L. (2024). Targeting lipid metabolism of macrophages: A new strategy for tumor therapy. J. Adv. Res. *85*, 85. https://doi.org/10.1016/j.jare.2024.02.009.
46. Wang, W., Li, T., Cheng, Y., Li, F., Qi, S., Mao, M., Wu, J., Liu, Q., Zhang, X., Li, X., et al. (2024). Identification of hypoxic macrophages in glioblastoma with therapeutic potential for vasculature normalization. Cancer Cell *42*, 815–832.e12. https://doi.org/10.1016/j.ccell.2024.03.013.
47. Wang, B., Wang, Y., Sun, X., Deng, G., Huang, W., Wu, X., Gu, Y., Tian, Z., Fan, Z., Xu, Q., et al. (2021). CXCR6 is required for antitumor efficacy of intratumoral CD8(+) T cell. J. Immunother. Cancer *9*, e003100. https://doi.org/10.1136/jitc-2021-003100.
48. Hao, Y., Hao, S., Andersen-Nissen, E., Mauck, W. M., 3rd, Zheng, S., Butler, A., Lee, M. J., Wilk, A. J., Darby, C., Zager, M., et al. (2021). Integrated analysis of multimodal single-cell data. Cell *184*, 3573–3587.e29. https://doi.org/10.1016/j.cell.2021.04.048.

STAR★METHODS

KEY RESOURCES TABLE

REAGENT or RESOURCE	SOURCE	IDENTIFIER
Antibodies		
Anti-mouse CD45.2-AF700 (Clone: 104)	BioLegend	Cat# 109822; RRID: AB_493731
Anti-mouse CD3ε-FITC (Clone: 17A2)	BioLegend	Cat# 100204; RRID: AB_312661
Anti-mouse 2B4-FITC (Clone: 2B4)	BD Pharmingen	Cat# 561778; RRID: AB_10893996
Anti-mouse CD8a-PE (Clone: 53–6.7)	BioLegend	Cat# 100708; RRID: AB_312747
Anti-mouse CD19-PerCP-Cy5.5 (Clone: 1D3)	BioLegend	Cat# 152406; RRID: AB_2629815
Anti-mouse NK-1.1-PerCP-Cy5.5 (Clone: PK136)	BioLegend	Cat# 108728; RRID: AB_2132705
Anti-human/mouse CD11b-PerCP-Cy5.5 (Clone: M1/70)	BioLegend	Cat# 101228; RRID: AB_893232
Anti-mouse CD279 (PD-1)-APC (Clone: RMP1-30)	BioLegend	Cat# 109112; RRID: AB_10612938
Anti-mouse CD4-PE Texas Red (Clone: RM4-5)	eBioscience	Cat# MCD0417; RRID: AB_10373812
Anti-human/mouse Granzyme B- Pacific Blue (Clone: GB11)	BioLegend	Cat# 515408; RRID: AB_2562196
Anti-mouse CD8a-FITC (Clone: 53–6.7)	BioLegend	Cat# 100706; RRID: AB_312745
Anti-mouse IFNγ-APC (Clone: XMG1.2)	BioLegend	Cat# 505810; RRID: AB_315404
Anti-mouse CD3ε-PerCP-Cy5.5 (Clone: 145-2C11)	BioLegend	Cat# 100328; RRID: AB_893318
Anti-mouse CD107a-PE-Cy7 (Clone: 1D4B)	BD Pharmingen	Cat# 560647; RRID: AB_1727419
Anti-mouse CD366 (TIM-3)-APC (Clone: RMT3-23)	BioLegend	Cat# 119706; RRID: AB_2561656
Anti-mouse CD244.2 (2B4)-PE (Clone: m2B4 (B6)458.1)	BioLegend	Cat# 133508; RRID: AB_2072855
Anti-mouse CD279 (PD-1)-PE/Cyanine7 (Clone: RMP1-30)	BioLegend	Cat# 109109; RRID: AB_572016
Anti-mouse TNF-α-APC-Cy7 (Clone: MP6-XT22)	BioLegend	Cat# 506343; RRID: AB_2565952
Anti-mouse Arginase 1-PE (Clone: A1exF5)	Invitrogen	Cat# 12-3697-82; RRID: AB_2734839
Anti-mouse CD206 (MMR)-APC (Clone: C068C2)	BioLegend	Cat# 141708; RRID: AB_10900231
Anti-mouse/human CD11b-APC-Cy7 (Clone: M1/70)	BioLegend	Cat# 101226; RRID: AB_830642
Anti-mouse TCR β chain-Brilliant Violet 605 (Clone: H57-597)	BioLegend	Cat# 109241; RRID: AB_2629563
Anti-mouse F4/80-FITC (Clone: BM8)	BioLegend	Cat# 123107; RRID: AB_893500
PE-Rat IgG2a, κ (Clone: RTK2758)	BioLegend	Cat# 400508; RRID: AB_326530
APC-Cy7- Rat IgG1, κ (Clone: RTK2071)	BioLegend	Cat# 400422; RRID: AB_830905
PE-Cy7- Rat IgG2b, κ (Clone: RTK4530)	BioLegend	Cat# 400617; RRID: AB_326559
APC-Rat IgG1, κ (Clone: RTK2071)	BioLegend	Cat# 400411; RRID: AB_326517
PE-Cy7-Rat IgG2a, κ (Clone: R35-95)	BD Pharmingen	Cat# 552784; RRID: AB_394465
FITC-Mouse IgG2b, κ (Clone: 27–35)	BD Pharmingen	Cat# 555057; RRID: AB_395677
APC-Rat IgG2b, κ (Clone: RTK4530)	BioLegend	Cat# 400612; RRID: AB_326556
Pacific Blue™-Mouse IgG1, κ (Clone: MOPC-21)	BioLegend	Cat# 400131; RRID: AB_2923473
PE-Mouse IgG1, κ (Clone: MOPC-21)	BioLegend	Cat# 400111; RRID: AB_2847829
PE-Cy7-Rat IgG2b, κ (Clone: RTK4530)	BioLegend	Cat# 400618; RRID: AB_326560
Anti-CD16/32 (Clone: 2.4G2; Fc blocker)	Lab generated	N/A
InVivoMAb rat IgG2b isotype control, anti-trinitrophenol (Clone: LTF-2)	Bio X Cell	Cat# BE0090; RRID: AB_1107780
InVivoMAb anti-mouse PD-1 (CD279) (Clone: RMP1-14)	Bio X Cell	Cat# BE0146; RRID: AB_10949053
Chemicals, peptides, and recombinant proteins		
Dulbecco's phosphate-buffered saline	Corning	Cat# 21-031-CVC
Dulbecco's Modified Eagle Medium	Corning	Cat# 10-013-CVRC
Fetal bovine serum, premium, United States origin	Corning	Cat# 35-015-CV

(*Continued on next page*)

Continued

REAGENT or RESOURCE	SOURCE	IDENTIFIER
Bovine Serum	Gibco	16170–078
Penicillin-streptomycin (100X)	GenDEPOT	CA-005-010
RPMI1640	Corning	10-040-CVRC
Propidium Iodide solution	BioLegend	421301
7-AAD	BioLegend	420404
Percoll	GE Healthcare	17-0891-01
Ionomycin calcium salt	Sigma	Cat# I3909
GolgiStop protein transport inhibitor (monensin)	BD Biosciences	Cat# 554724
GolgiPlug protein transport inhibitor (Brefeldin A)	BD Biosciences	Cat# 555029
Cytofix/Cytoperm fixation and permeabilization solution	BD Biosciences	Cat# 554722
Zombie Aqua Fixable Viability Kit	BioLegend	Cat# 423102
Fixable viability Stain 450	BD Biosciences	Cat# 562247
Fixable viability dye 780	BD Biosciences	Cat# 565388
Critical commercial assays		
Chromium Single Cell 3′ reagent Kits v3	10X Genomics	
Agilent High Sensitivity DNA kit	Agilent	5067–4626
HiSeq X Ten Reagent Kit v2.5	Illumina	FC-501-2501
PhiX Control v3	Illumina	FC-110-3001
Deposited data		
scRNAseq raw data	This manuscript	GSE264251
Experimental models: Cell lines		
Mouse: GL261	Dr. Injune Kim (KAIST)	N/A
Experimental models: Organisms/strains		
Mouse: B6.129S2- *Ifnar1*^{tm1Agt}/Mmjax	The Jackson Laboratory	MMRRC Strain #032045-JAX; RRID: MMRRC_032045-JAX
Mouse: C57BL/6J	KAIST	https://spf.kaist.ac.kr/
Mouse: C57BL/6J	DBL. Co. Ltd	http://www.dbl.kr/bbs/board.php?tbl = animal&chr = &category = %2C%27DBL+%EC%83%9D%EC%82%B0%EB%8F%99%EB%AC%BC%27&findType = &findWord = &sort1 = &sort2%20 = %20
Software and algorithms		
R statistical programming environment v. 4.2.1	R Core	https://www.r-project.org
Cell Ranger 3.1.0	10X Genomics	
R studio		https://rstudio.com
Seurat_4.1.0	(Hao et al., 2021)[48]	https://satijalab.org/seurat/
GSEA software v.4.0.3	GSEA	https://www.gsea-msigdb.org
FlowJo v.10.5.3	Treestar	https://www.flowjo.com/solutions/flowjo/downloads
Prism software v.9.0	Graphpad	https://www.graphpad.com/scientific-software/prism/

(*Continued on next page*)

Continued

REAGENT or RESOURCE	SOURCE	IDENTIFIER
Other		
CellDropTM Automated Cell Counter	DeNovix	CellDrop FL-UNLTD
Digital mouse stereotaxic frame	World Precision Instruments	505314
Animal Anesthesia Vaporizers type 1	RWD	R580S
Syringe Pump	KD Scientific	LEGATO 130
Hamilton Syringe	Hamilton	803
HiSeq X Ten	Illumina	
MiniAmp Thermal Cycler	Thermo Fisher Scientific	A37834
Chromium Controller	10X Genomics	
2100 Bioanalyzer	Agilent	G2939BA
LSRFortessa^{TM} X-20 Cell Analyzer	BD Biosciences	
FACSAria II	BD Biosciences	
Micro Drill	SAESHIN	
Petroff-Hauser chamber	Fisher Scientific	267113

EXPERIMENTAL MODEL AND STUDY PARTICIPANT DETAILS

Mice

C57BL/6J mice between 8 and 13 weeks of age at the time of Gl261 tumor implantation were used. Unless otherwise noted, all mice were bred in a specific pathogen free facility of the KAIST Laboratory Animal Resource Center with no more than five mice per cage. C57BL/6J mice were purchased from KAIST and DBL Co. Ltd (Eumseong, Korea). All procedures were performed according to the guidelines and protocols of KAIST's Institutional Animal Care and Use Committee (IACUC) and were approved by the IACUC (KA2024-026).

Tumor cell lines

The Gl261 mouse glioma cell lines were provided by Professor Injune Kim of KAIST. The mouse tumor cell line was cultured in a cell culture flask with 1% penicillin/streptomycin (GenDEPOT, USA) and 10% fetal bovine serum (Corning, NY, USA) added to Dulbecco's Modified Eagle Medium (DMEM, Corning, NY, USA) at 37°C with 5% CO_2. The absence of mycoplasma contamination was confirmed in the cell line used for the experiment using a Mycoplasma PCR kit (Intron Biotechnology, Seongnam, Korea). Cells were dissociated using trypsin-ethylenediaminetetraacetic acid (EDTA) (Corning).

METHOD DETAILS

Syngeneic mouse glioblastoma model

To induce GBM in the mouse brain, we used an orthotopic glioma injection model by inoculating the brain with the mouse glioma cell lines mentioned above. Each mouse was implanted with 1 x 10^5 Gl261 cells. Gl261 cells were removed from the cell culture flask using trypsin-EDTA, neutralized with DMEM, and then washed with Dulbecco's phosphate-buffered saline (DPBS). Cells were diluted to 10^5 cells/2μL in DPBS and stored on ice until inoculation in the brain.

For tumor cell implantation, mice were anesthetized with isoflurane and fixed on a stereotaxic instrument (Stoelting Co, Wood Dale, IL, USA). Ophthalmic ointment was applied to the eyes to protect from dryness and damage. The scalp was first sterilized with alcohol and a midline incision was made in the skin and opened to expose the top of the skull. A small hole was drilled in the skull 2 mm to the right and 2 mm anterior from the bregma and Gl261 tumor cells were loaded into a Hamilton syringe (The Hamilton Company, Reno, NV, USA) and injected 3 mm beneath the brain surface for 5 min at a rate of 0.4μL/min with a nano-injector (KD Scientific, Holliston, MA, USA). After injection, the drilled hole was closed with adhesive glue and the skin was sutured using a synthetic multifilament absorbable suture.

Analysis of human GBM patient data

The TCGA-GBM and TCGA-LGG study data was processed using the Gene Expression Profiling Interactive Analysis (GEPIA) platform. For single-cell RNA sequencing analysis of newly diagnosed GBM patient, we used data from a previous study (GSE182109).

Tumor digestion and single cell isolation

Mice were euthanized via a CO_2 gas chamber and transcardially perfused with cold DPBS to remove blood before isolating tissues. All brains were mechanically and enzymatically digested using the Tumor Dissociation Kit (Miltenyi Biotec, 130-096-730) in a gentleMACS C tube

(Miltenyi Biotec) and then dissociated with a gentleMACS OctoDissociator using program 37C_mTDK_1 for 40 min, followed by filtration with 70 μm cell strainers. The resulting cell suspensions were loaded onto a 30%/70% Percoll gradient (GE Healthcare, Chicago, IL) and centrifuged. After harvesting the immune cells at the interface of the two Percoll layers, the cells were incubated in ACK lysis buffer at room temperature for 5 min to remove the remaining red blood cells.

QUANTIFICATION AND STATISTICAL ANALYSIS

Flow cytometry

Single-cell suspensions were treated with an anti-CD16/32 antibody (2.4G2) to block Fc receptors prior and stained with antibody mixture against the following surface molecules: CD45.2 (clone:104), 2B4 (clone:2B4), CD19 (clone:1D3), CD11b (clone:M1/70), CD279 (clone: RMP1-30), CD4 (clone:RM4-5), CD8α (clone:56–6.7), CD366 (clone: RMT3-23), F4/80 (clone: BM8). To stimulate immune cells for cytokine production, we cultured single-cell suspensions in RPMI complete medium with 50 ng/mL phorbol-myristate acetate (Sigma), 1 μg/mL ionomycin (Sigma), 1μM GolgiPlug (BD Biosciences), and 1μM GolgiStop (BD Biosciences) for 4 h at 37°C. Cells were fixed and permeabilized using the BD Cytofix/Cytoperm Fixation/Permeabilization Kit (BD Biosciences, 554714) according to the manufacturer's recommended protocol. Antibodies against the following proteins were used for intracellular cytokine staining: IFN-γ (clone: XMG1.2), TNF-α (clone: MP6-XT22), CD107a (clone: 1D4B), and Granzyme B (clone: GB11). For intracellular staining of Arginase 1 (clone: A1exF5) and CD206 (clone: C068C2), cells were treated with GolgiPlug (BD Biosciences) diluted in complete RPMI at 1:1000 and GolgiStop (BD Biosciences) diluted in complete RPMI at 1:1500 for 4 h at 37°C. Fixable viability dye 450 (eBioscience, 65-0863-14), Zombie Aqua Fixable Viability Kit (BioLegend, 423101), and 7-aminoactinomycin (7-AAD) (BD, 51-68981E) was used to discriminate between live and dead cells. All samples were acquired using an LSRFortessa flow cytometer (BD), and the data were analyzed using FlowJo software 10.5.3 (Treestar).

Single-cell RNA sequencing

On day 20 following Gl261 injection, single-cell suspensions were prepared from the brain as described above. Suspensions were pooled into one sample from five mice in each group. The single-cell suspensions were treated with an anti-CD16/32 antibody (2.4G2, Fc blocker) to block Fc receptors prior to staining with mouse-specific antibodies. The cells were stained with CD45.2 (clone: 104) to distinguish for immune cells. Live immune cells were isolated using a FACS Aria II (BD Biosciences) flow cytometer, and 7-AAD staining was performed to discriminate between live and dead cells.

For analysis of brain immune cells following anti-PD1 treatment, single-cell suspensions were prepared from the brains on day 25 following Gl261 injection. Suspensions were pooled and treated with Fc blocker as mentioned above. Cells were stained with CD45.2 (clone:104) and CD3ε (clone: 17A2) to distinguish for $CD3^+$ T cells. Fixable viability dye 780 (565388, BD) was used to discriminate between live and dead cells.

The 10X chromium single cell 3′ library kit (10X Genomics, Pleasanton, CA, USA) was used to generate a single cell library. Samples were sequenced with HiSeqXten (Illumina, San Diego, CA, USA) for 10,000 cells. A Chromium Single Cell 3′ Reagent kit (version 3; 10X Genomics) was used for scRNA-seq according to the manufacturer's recommended protocol. Sorted cells were loaded with gel beads for emulsion generation and barcoding, cDNA was amplified, and libraries were constructed. Next-generation sequencing was performed with the HiSeqXten (Illumina) platform for 10,000 cells per pooled sample. The sequencing results were converted into FASTQ files using Cell Ranger (10X Genomics), and sequences were aligned using the mouse genome 10–3.0.0 (10X Genomics) as a reference.

Matrices were loaded into Seurat v4.1 for analysis and R 4.2.1 was used for statistical analysis. Cells with unique RNA features were excluded for quality control. Cells in which more than 5% of reads aligned to mitochondrial genes were also excluded. Changes in gene expression were identified using the FindVariablesFeatures function. Datasets for the WT and $IFN\alpha R^{-/-}$ groups were integrated using the FindIntegrationAnchors and IntegrateData functions. The data dimension was reduced using principal component (PC) analysis for each sample, and 20 significant PCs were identified. Data were clustered using the FindNeighbors and FindClusters functions at a resolution of 0.5. RunUMAP functions were used to visualize the selected PCs. The Seurat workflow was used to sort and visualize the normalized number of genes per cell. DEGs were identified using the FindMarkers functions. For GSEA analysis, DEGs were annotated on the reference gene set based on MSigDB 7.0.

NicheNet analysis

Ligand-receptor interactions between cell populations from scRNA dataset were performed using nichenetr package. Required data that include NicheNet networks and ligand-target matrix were loaded. NicheNet analysis was performed as described in (https://github.com/saeyslab/nichenetr/blob/master/vignettes/ligand_activity_geneset.md). Receiver was set to T cell cluster, in order to determine the cell types that contributed to changes in the gene expression profile. NicheNet analysis was carried out based on the differentially expressed genes in T cells using the FindMarkers function of Seurat package.

CellChat analysis

Cell-to-cell communication networks between immune cell populations were performed using Cellchat package. Required data that include information on cell signaling networks were loaded from CellchatDB. Further Cellchat analysis was performed as described in (https://htmlpreview.github.io/?https://github.com/jinworks/CellChat/blob/master/tutorial/CellChat-vignette.html).

Immune checkpoint blockade administration

For anti-PD1 administration, 200 μg of an InVivoMab anti-mouse PD-1 blocking antibody (BioXcell, BE0416) was diluted in 100 μL of DPBS and injected intraperitoneally into each mouse on days 7, 11, 15, and 19 after Gl261 tumor inoculation. As a control, InVivoMab rat IgG2a isotype antibody (BioXcell, BE0090) at the same concentration was injected.

All data are expressed as the mean ± standard error of the mean (SEM). Statistical analyses of differences between the two groups used an unpaired, two-tailed Student's t test. A comparison of survival rate was made with the log rank test. Prism 9.3.1 software (GraphPad, San Diego, CA, USA) was used for the statistical analysis. Statistically significant differences are indicated as follows: $*p < 0.05$, $**p < 0.01$, $***p < 0.001$, and $****p < 0.0001$.